Early Stages of RNA-Mediated Conversion of Human Prions

Emilia A. Lubecka[*,†] and Ulrich H.E. Hansmann[*,‡]

†*Faculty of Electronics, Telecommunications and Informatics, Gdansk University of Technology, G. Narutowicza 11/12, 80-233 Gdansk, Poland*

‡*Dept. of Chemistry & Biochemistry, University of Oklahoma, Norman, OK 73019,USA*

E-mail: emilubec@eti.pg.edu.pl; uhansmann@ou.edu

Abstract

Prion diseases are characterized by the conversion of prion proteins from a PrP^C fold into disease-causing PrP^{SC} form that is self-replicating. A possible agent to trigger this conversion is poly-adenosine RNA, but both mechanism and pathways of the conversion are poorly understood. Using coarse-grained molecular dynamic simulations we study the time evolution of PrP^C over 600 μs. We find that both the D178N mutation and interacting with poly-adenosine RNA reduce the helicity of the protein and encourage formation of segments with strand-like motifs. We conjecture that these transient β-strands nucleate the conversion of the protein to the scrapie conformation PrP^{SC}.

1 INTRODUCTION

Various proteins can form disease-causing aggregates after misfolding. In some cases do the misfolded proteins or aggregates propagate by recruiting folded or unfolded proteins and subsequently changing the structure of these proteins into their own. This infectious nature of mis-folded and amyloid forming proteins is best established for prions. Here, the disease-causing PrP^{SC} form can convert unfolded prions, or such in a native PrP^{C} state, into their own form.[1] In turn, this self-replication increases the chance that the mis-folded PrP^{SC} assemble in a second step into cell-toxic aggregates, which in humans may cause neurodegenerative diseases such as Creutzfeldt-Jacob or Kuru.[2] Various mutations can alter the speed of nucleation changing onset and severity of the symptoms. An example is the heritable mutation D178N, replacing an acidic aspartic acid (D), by a neutral asparagine (N). This mutation is implied in fatal familial insomnia where a loss of neurons in the thalamus[3] progressively worsens insomnia and eventually leads to dementia.[4] Note that symptoms of fatal familial insomnia appear only if the prion has methionine (M) at position 129 and is not observed with a valine (V) at position 129, another variant often found in the wild type.[5] Nucleation of the initial seed may also be enhanced by environmental conditions or interaction with other molecules. For instance, various studies by us and other groups point to the possibility that poly-adenosine RNA (poly-A-RNA) catalyzes conversion of the native PrP^{C} form into PrP^{SC}.[6–9]

However, the predictive power of our previous studies is limited by the short time scales of our simulations. Covering only 300 ns, our simulations allowed us only to investigate early steps in the conversion between PrP^{C} and PrP^{SC}, a process that *in vivo* requires minutes to hours. This discrepancy of time scales between the biological process and what can be simulated in all-atom simulations is a common hurdle in computational biophysics and biochemistry. While the problem can often be alleviated by the use of enhanced sampling

techniques such as replica exchange and other generalized ensemble techniques,[10–12] such an approach fails in our case. This is because these enhanced sampling techniques rely on an artificial dynamics and therefore are not suited for investigating directly the dynamics of the conversion between PrP^C and PrP^{SC}. Another possibility to reduce the computational difficulties is coarse-graining. Lowering the resolution of the system allows for larger time steps,[13,14] but requires a careful calibration of the energy. This is because the smaller number of degrees of freedom lowers the entropy of the system, which needs to be compensated by modifying the enthalpy contributions. One successful example of coarse-grained force fields is UNRES, which has been shown to cover biomolecular processes of proteins on time scales rarely possible in all-atom simulations.[15] Numerous previous applications include studies ofprotein folding[16] and studies of the mechanism of the formation of oligomers and fibrils of amyloidogenic peptides.[17–19] When merged with similar coarse-grained force fields for nucleic acids (NARES-2P),[20] the force field is called UNIfied COarse gRaiNed model (UNICORN),[15,21] and has been recently also extended to treat protein-nucleic-acid complexes.[22]

Hence, in the present paper we use coarse-grained simulations relying on UNRES/NARES-2P to revisit the question of how presence of poly-adenosine RNA alters the conversion between PrP^C and PrP^{SC} in both wild type and fatal familial insomnia causing mutants. As in our earlier work we study wild type versions with a methionine or a valine as residue 129 (129M-178D and 129V-178D) and the corresponding mutants (129M-178N and 129V-178N). The four variants of human prions are simulated both with and without presence of poly-A-RNA, i.e., eight different systems. While connecting in this way to our earlier work, the use the coarse-grained simulations allows us to cover 600 μs, i.e., a time span that is 2000 times longer than the one considered by us in Ref.[9] Comparing the various systems, we find that both the D178N mutation and interacting with poly-adenosine RNA reduce the helicity of the protein and encourage formation of transient β-strands.As was already conjectured in

4

earlier studies,[23,24] such strands are likely the seed for the conversion into the β-sheet rich PrP^{SC} form.

2 MATERIALS AND METHODS

2.1 Model Preparation

We have considered four systems: the wild type human prion protein with either residue 129 a methionine (129M) or a valine (129V) and residue 178 an aspartic acid (178D), with the two variants referred to as (129M-178D) and (129V-178D); and the two mutants (129V-178N) and (129M-178N) where residue 178 is anasparagine (178N) instead of an aspartic acid. Our models are derived from the X-ray-resolved PrP^{C} structure for the wild type variant (129M-178D), as deposited in the Protein Data Bank (PDB) under PDB-ID: 2LSB. In the other models are the side chains of residue 129 and/or residue 178 replaced accordingly to derive the alternate wild type variant or one of the two mutants, with the new side chains initially in the standard configuration and minimized to fit into the geometry of the PDB structure. As only the C-terminus of the prion has been resolved, we have used I-TASSER[25,26] and MODELLER[27] to predict a structure for the unresolved N-terminal segment of residues 1-121. Specifically, we have generated five conformations for each of the four full-sized systems and minimized, using AMBER16.[28] Based on energy, we then selected one model for each system for the docking with RNA and for the control simulations. Note that we consider in this study only unanchored prions, i.e., ignoring the glycosylphosphatidylinositol (GPI) anchor with which prions attach to cell membranes in humans.

The 6-nucleotide RNA was created with the LEAP module of the AMBER16[28] followed by a short energy minimization, and docked to each of the four systems using AutoDock Viena[29] to generate the poly-A-RNA - protein complexes. The 10 highest scoring docked systems for each of the four targets were collected and examined for common regions of

protein-RNA interaction. As in our previous studies[9,30] we found three main binding sites: binding site 1 (residues 21-31), binding site 2 (residues 111-121) and binding site 3 (residues 144-155). For the wild type 129M-178D and the mutant 129V-178N all three binding sites were found, while in the wild-type variant 129V-178D binding site 3 is lost, and in the mutant 129M-178N the binding sites 1 and 2 are lost. Hence, in total we have studied nine poly-A-RNA-protein complexes: three for 129M-178D, two for 129V-178D, one for 129M-178N and three for 129V-178N. These complexes and the corresponding controls (the prions without poly-A-RNA binding to it) are listed in Table 1.

2.2 Simulation Protocol

Both the poly-A-RNA -prion complexes and the control were studied in UNRES/NARES-2P coarse-grained molecular dynamics simulations. In order to compare our results with previous work, and to ensure that the coarse-grained simulations do not introduce a bias, we have studied also the 129M-178D wild type variant in all-atom molecular dynamics simulations, using the ff14SB[31] (for proteins) and ff-DNA-bsc1-OL15[32] (for nucleic acids) force fields as implemented in the AMBER16 package.[28] A matrix of the various systems, binding sites, and trajectory numbers is given in Table 1.

Table 1: Number and lengths of trajectories run for the simulated systems.

| force field | system | RNA binding site | | | without RNA |
		site 1	site 2	site 3	
AMBER[a]	129M-178D	-	-	3	1
UNRES/NARES-2P[b]	129M-178D	8	8	8	8
	129V-178D	8	8	-	8
	129V-178N	8	8	8	8
	129M-178N	-	-	8	8

a - each trajectory was 1,500 ns long;
b - each trajectory consisted of 125,000,000 steps with 4.89 fs step length, which is 611.25 ns UNRES time, and about 600 μs real time.

6

The coarse-grained simulations are carried out with the UNRES (for proteins) and NARES-2P (for nucleic acids) force fields.[22] The following NARES-2P force fields weights were optimized: (1) $W_{SC-BASE}$ - protein side-chain (SC) interaction with nucleobase (BASE); (2) W_{SC-PHO} - protein side-chain (SC) interaction with phosphate group (PHO); (3) $W_{PEP-PHO}$ - protein peptide group (PEP) interaction with phosphate group (PHO); and (4) $W_{PEP-BASE}$ - protein peptide group (PEP) interaction with nucleobase (unpublished results). The final weights values used were: 3.2, 0.4, 0.1 and 0.1, for $W_{SC-BASE}$,W_{SC-PHO}, $W_{PEP-PHO}$ and $W_{PEP-BASE}$, respectively.

We have run molecular dynamic simulations with UNRES/NARES-2P for the 13 systems listed in Table 1: the wild type 129M-178D (with RNA bound to either binding site 1, 2 or 3), the 129V-178D wild-type variant (RNA bound to either site 1 or 2), the 129M-178N mutant (with binding site 3), the 129V-178N mutant (with RNA bound to either of the three binding sites), and the corresponding four controls. For the prion-RNA complexes we have selected as start conformations the ones obtained with AutoDock that gave the highest docking score. All nine prion-RNA complexes and the corresponding four controls (the prion variants in absence of RNA), were energy minimized in 500 steps. The time evolution of each of these 13 start configurations was followed in eight independent UNRES/NARES-2P molecular dynamics trajectories. The eight trajectories for each of the 13 systems differ in the initial velocity distribution, randomly generated corresponding to a temperature of 300 K, and evolve with a Langevin dynamics, using a Velocity-Verlet integrator with the Adaptive Multiple Time Step (A-MTS) algorithm[33] for integrating the equations of motion. Water friction is scaled by the factor of 0.01 in the computation of the friction and stochastic forces.[34] Each trajectory consisted of 125,000,000 steps with 4.89 fs step length leading to 611.25 ns in UNRES time. However, the UNRES time scale is not a physical one, and one UNRES time step corresponds to about 1000 steps on a "physical" time scale,[34] i.e., about 600 μs of physical time are covered in each trajectory. Snapshots are collected every 5,000s

7

steps for further analysis. Secondary structure in UNRES is detected based on peptide-group contacts, as specified in ref,[35] and using keywords HELIX and SHEET is written directly in the Protein Data Bank (PDB) format into output files (calculated using distances and peptide group orientation).

The purpose of our all atom-simulations of the wild type 129M-178D is to exclude force field bias in our UNRES simulations and to double-check the time conversion factor. Again, we have selected as start points of the trajectories the complexes with the highest docking score and use as control the prion protein without poly-A-RNA. Using the LEAP module of AMBER16,[28] both control and the complex are solvated in a truncated octahedral periodic box of 15 Å side length, filed with TIP3 water molecules,[36] and neutralized by counter ions. This procedure leads to a total of about 64,000 atoms for each of the systems. After short energy minimization each system is equilibrated at 300 K for 2 ns at constant volume followed by additional 2ns at constant pressure. For data generation, the system were simulated for 1,500 ns at 300K and constant volume. By constraining bonds involving hydrogen with the SHAKE algorithm[37] we are able to use a time step of two fs. Because of the use of periodic boundary conditions we use the Particle-mesh Ewald (PME) procedure[38] for calculating electrostatic interactions beyond a cut-off radius of 8 Å. The coordinates were collected every 25,000th step. No external constraints are applied in our molecular dynamics simulations, performed using AMBER16 and PMEMD CUDA.[28,39,40] For our analysis we have considered only complexes where we did not observe RNA detachment at early stages of the trajectories. This left us with three RNA-prion trajectories which together with the control are analyzed using the Ptraj program from the AMBER16 package.[28]

3 RESULTS AND DISCUSSION

3.1 Validating UNRES coarse-grained simulations against AMBER all-atom simulations

Previous studies, relying on all-atom simulations of a few hundred ns, could only cover the earliest steps in RNA-mediated conversion of prions.[9,30,41] In this work, we use the UNRES coarse-grained force field to extend this time span by three orders of magnitude. UNRES has been extensively tested and shown to lead to a 4000-fold speedup over all-atom simulations relying on the AMBER force field,[34] We first confirm a previous observation that a single time step in UNRES corresponds to more than 1000 fs in AMBER all-atom simulations. For this purpose, we compare for the 129M-178D wild type AMBER all-tom trajectories of 1,500 ns length with the initial parts of the the corresponding UNRES coarse-grained simulations. Assuming the scaling factor of 1000, this amounts to 1.5×10^6 UNRES time steps. AMBER is chosen as all-atom force field for this comparison as parts of UNRES (for instance, the UNICORN potentials[42] for the interactions between proteins and DNA,[43] and backbone-local potentials of O1→4-bonded polyglucose chains in SUGRES-1P[44]), were parametrized on AMBER simulations, and therefore there is usually good agreement between UNRES and all-atom AMBER simulations.[20,45]

Our comparison of simulations using the two force fields is done for both the isolated prion and for the prion interacting with RNA bound to site 3. The resulting time evolution of secondary structure in coarse-grained and all-atom simulations resemble each other, as can be seen in Fig. 1, where we show the measured helicity as function of time in Fig. 1 (a) and (b), and presence of β-strands in Fig. 1 (c) and (d). While not shown here, we note that the C^α-root mean square deviation (RMSD) of the final configuration with respect to the start configuration behaves in a similar way. For example, we measure for the C-terminal domain (residues 121-253) of the prion bound to RNA a value of 6.7 (+/- 0.7) Å in the all-atom
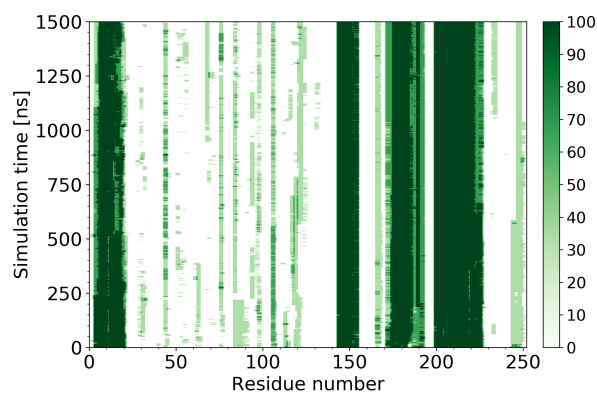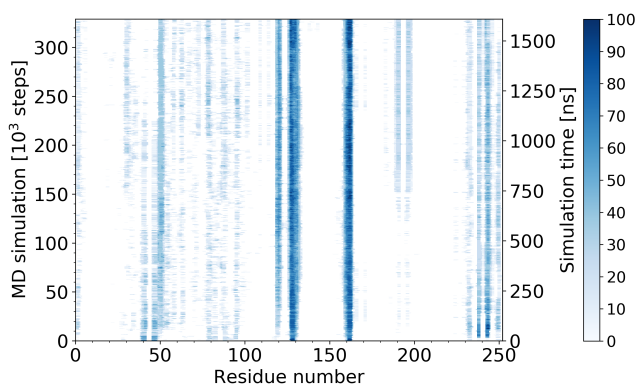
(a) AMBER - helicity [%]
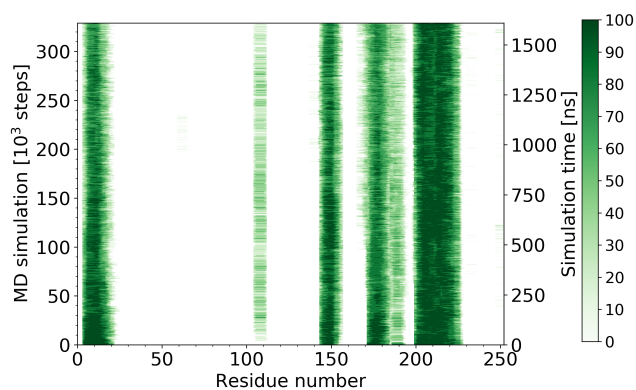
(b) UNRES/NARES-2P - helicity [%]
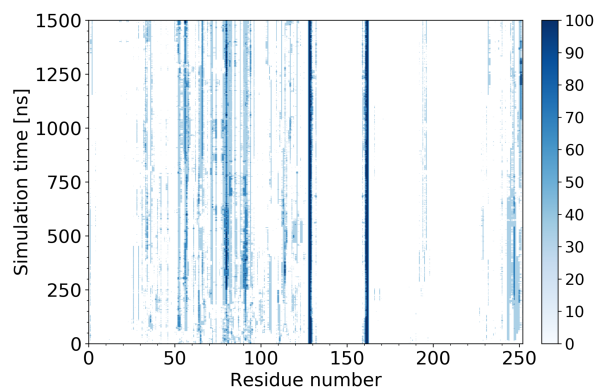
(c) AMBER - β-structure [%]

(d) UNRES/NARES-2P - β-structure [%]

Figure 1: Time evolution of secondary structure as measured for the 129M-178D prion-RNA complex secondary structure in all-atom (AMBER) simulations (a and c), and in coarse-grained (UNRES) (b and d) simulations. The helical fragments are marked in green colors (a and b), and the β-strands in blue (c and d). The colors intensity corresponds to the frequency of occurrence of the secondary structure. All trajectories start with RNA bound to the binding site 3 of the wild type 129M-178D prion.

10

(AMBER) simulations, and 7.5 (+/- 1.2) Å in the UNRES coarse-grained simulations. Here, the averages are taken over the respective trajectories, see Table 1. Hence, despite using a highly-reduced model, the time evolution of the prion (or prion-RNA complex) appears to be similar in the UNRES and in the AMBER simulations. In addition, the RMSD values are also similar to the ones seen in our earlier work in Ref.[9] which relied on 300 ns long all-atom simulations using the CHARMM force field. As in this previous work, we see in both UNRES and AMBER simulations the formation of the RNA encapsulating pincer motif between the poly-basic domains of residues 21-31 and residues on helix A, however shifted from residues 144-148 to residues in the interval 150-160. And while unlike in our earlier work,[30] helix A does not unfold, it does become less stable. This deviation in stability likely reflects the differences in the two all-atom force fields: the AMBER force field is known for its stabilization of helices, while CHARMM36 was developed considering also intrinsically disordered proteins.[46] Hence, as the differences between the AMBER all-atom and the UNRES coarse-grained simulations are comparable to that seen between AMBER and CHARMM simulations, we conclude that use of the coarse-grained UNRES force field does not introduce obvious biases into our study. This gives us confidence in the reliability of our UNRES coarse-grained simulations. In fact, we believe that force-field induced over-stabilization of secondary structure is less of a problem for UNRES than for AMBER as the UNRES simulations cover much larger time scales.

3.2 The effect of poly-A-RNA and sequence variations on prion stability

In the last section, we have verified that for time scales, where a comparison between coarse-grained UNRES and the all-atom simulations is still doable, the time evolution of prions is similar in both sets of simulations. Observed differences are comparable to the ones seen
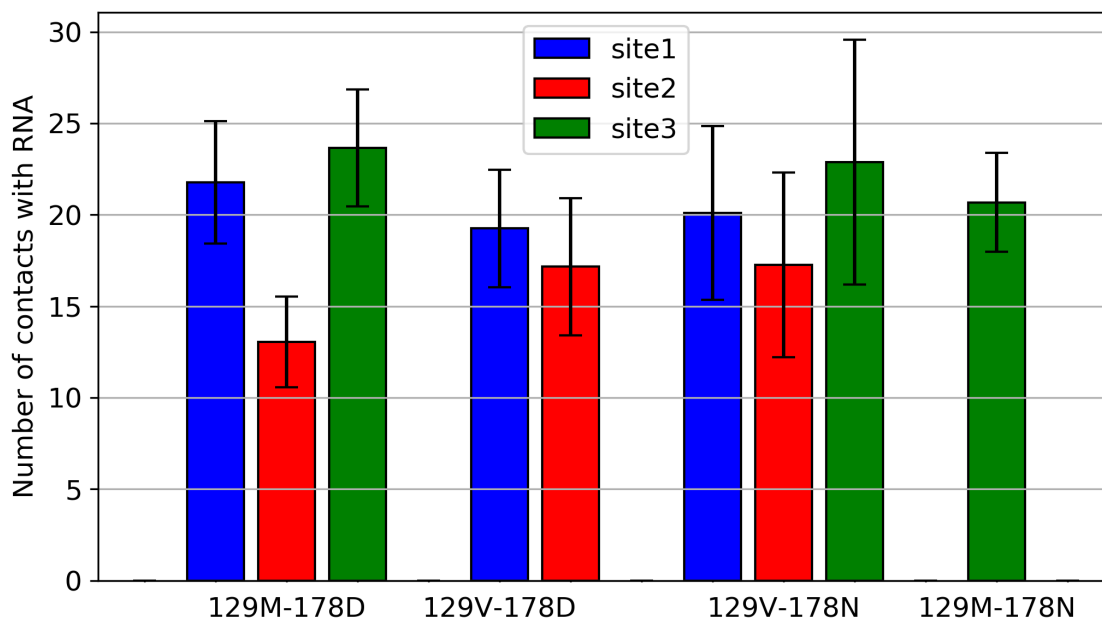
Figure 2: Average number of contacts between prion and RNA, measured for the last 120 μs of the 600 μs and averaged over all eight trajectories of the corresponding systems. The error bars represent the standard deviation of the average.

between different all-atom force fields. This allows us to study the evolution of prions, and the effect of poly-A-RNA, over much longer time scales, in our case about 600 μs instead of the 1.5 μs covered in the above all-atom simulations. While this time range still too small to observe the conversion between the prevalent cellular conformation (PrP^C) and the scrapie conformation (PrP^{SC}), the thousand times larger time range allows a much deeper investigation into the early events of the conversion.
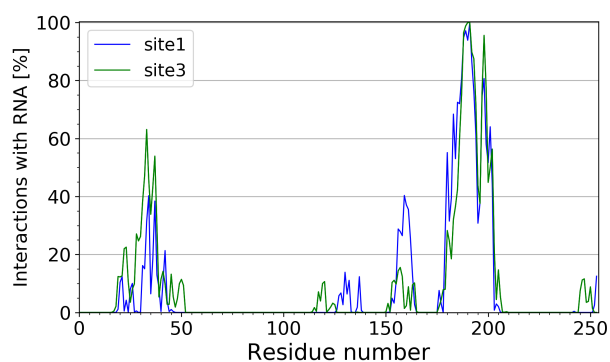
The first quantity that we study is the number of contacts between the poly-A-RNA fragment and the prion protein. This quantity, as measured for the last 120 μs is shown in in Fig. 2 for the four prion variants. Here, we define a contact by the requirement that the distance between a Cα-carbon atoms on prion protein and a C1' atom the RNA segment is smaller than 8 Å. For the 129M-178D wild type we find almost twice the number of contacts for binding site 1 and 3 (with an average number of contacts of 22 and 24, respectively) then seen for the binding site 2 (about 13 contacts). The differences are less pronounced

12

for the other three variants, but in each case where (guided by our previous work[30]) we have considered binding at site 2, we find a smaller number of contacts than seen at the other binding sites. When looking into the distribution of contacts, see Fig. 3, we observe for the 129M-178D wild type that for binding site 1 and 3 the RNA forms contacts with residues 21-31 and 150-161 (located on helix A), which along the trajectories extend later to residue 140-161 while also adding contacts with residues 41 and contacts with residues 180-200 located on helix B. Such pincer-like arrangement and a large number of contacts with residues located on helix B are also observed for 129V-178D and the two mutants when the RNA fragment binds to either site 1 or 3. This larger number of contacts and their pincer-like arrangement suggests a higher stability of the complex for binding sites 1 and 3 over that of binding to site 2, an observation that is consistent with our previous work.[9]
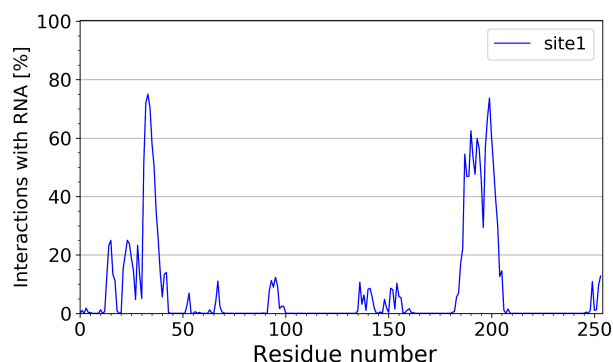
How does the binding of the RNA fragment affect the stability of the prion protein? In the functional form, PrP^C, the prion protein has three α-helices and a single short antiparallel β-sheet ($\beta1$: residues 129-130, and $\beta2$: 162-163, PDB-ID: 2LSB[47]). The conversion from the helix-rich (PrP^C) to the scrapie conformation rich with β-strands (PrP^{SC}) involves spontaneous partial unwinding of the helices and subsequent growth of strands in the prion. When comparing the average helicity and strandness, as measured in the last 120 μs in our runs, we observe in all cases a loss of helicity, see Fig. 4, which in absence of RNA is largest for the 129V-178N mutant. When the poly-A-RNA fragment binds to site 1 or 3, the loss in helicity is usually larger than in the control, or when binding to site 2. Hence, in the further discussion we focus on binding to site 1 and 3, and since both leading to pincer-like motif, we treat them as a single entity.

Note that even in absence of poly-A-RNA there is a loss of helicity for helices A, B and C in all four prion variants. For helix A, the helicity as measured over the last 120 μs, is about 50% of that in the start configuration for the wild type variants (with residue 178D), and less than 40% for the mutants (having 178N). Binding of poly-A-RNA to site 1 or 3 does
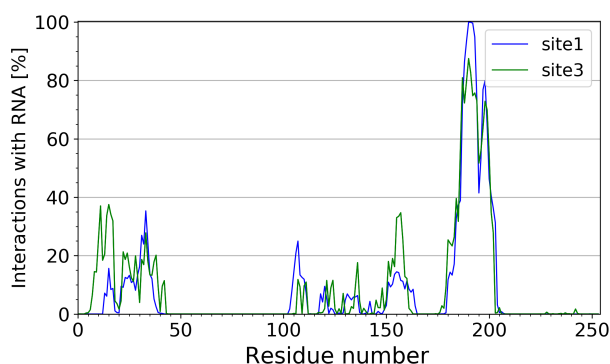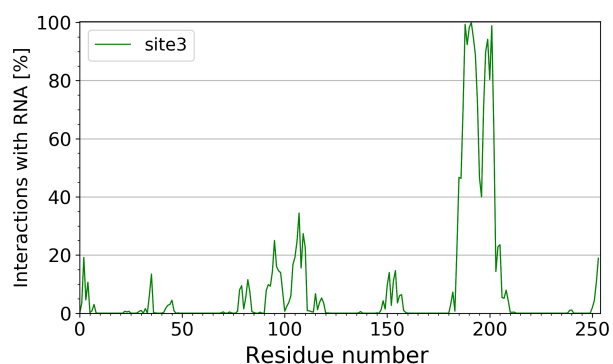
13

Figure 3: Frequency of contacts with the poly-A-RNA fragment for residue of the four prion systems, the two wild type variants : a) 129M-178D and b) 129V-178D; and the two mutants c) 129V-178N and d) 129M-178N. The contact frequency is show as percentage and calculated over the last 120 μs, averaged over all eight trajectories for each system.
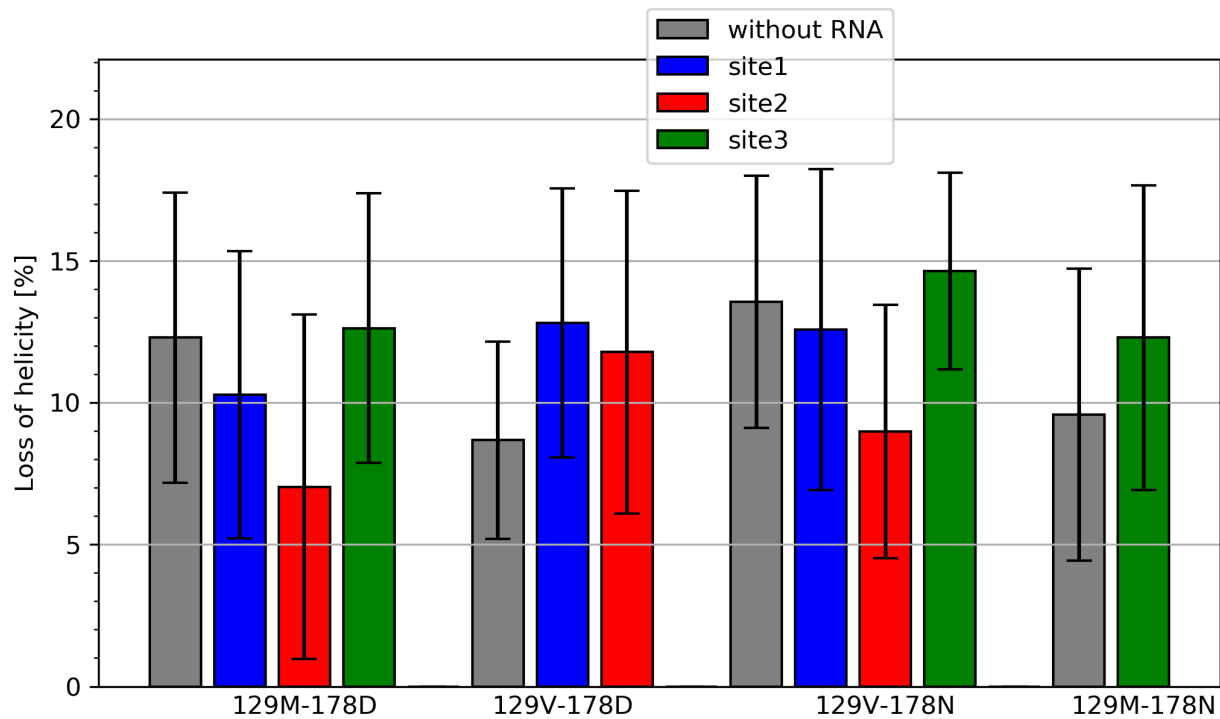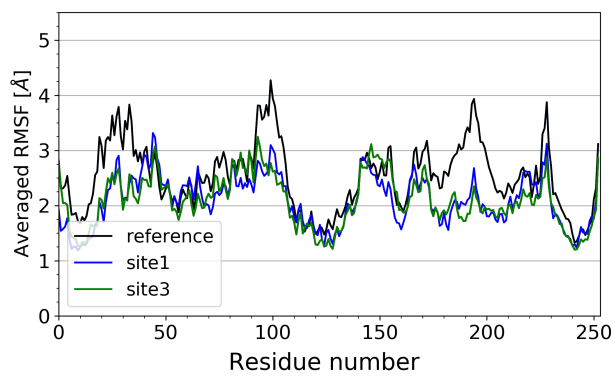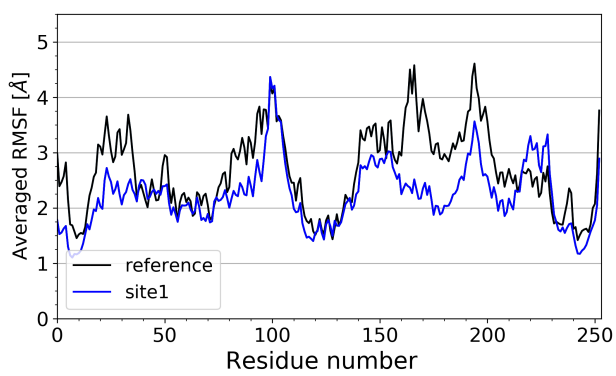
Figure 4: The loss of total helicity of the prion in regard to the start configuration, as measured for each system for the last 120 μs and average over eight trajectories. The total helicity is calculated for the C-terminal domain (residues 121 to 253).[30] The error bars represent the standard deviation.

(a) 129M-178D

(b) 129V-178D
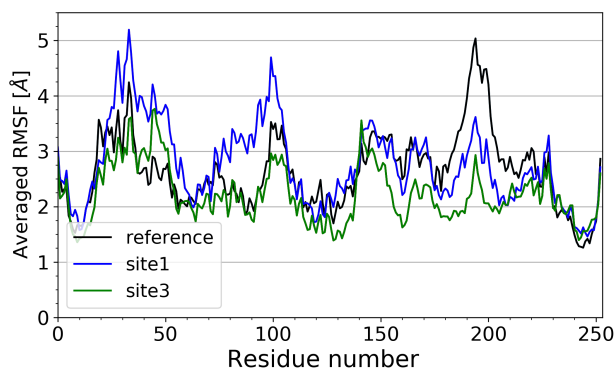
(c) 129V-178N

(d) 129M-178N

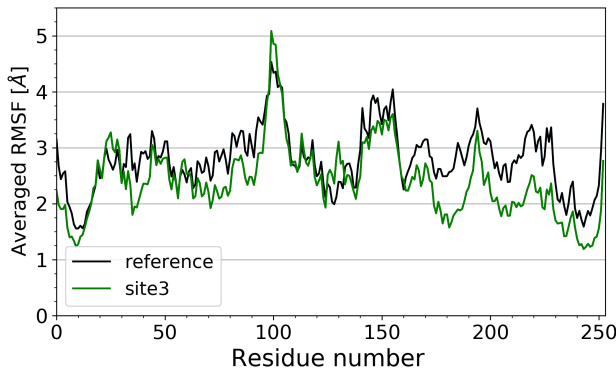Figure 5: Root-mean-square-fluctuation (RMSF) measured over the last 120 μs and averaged over eight trajectories, for residue of the four prion systems, the two wild type variants: a) 129M-178D and b) 129V-178D; and the two mutants: c) 129V-178N and d) 129M-178N.

16

not change these numbers. Visual inspection of the trajectories shows that this reduction in helicity reflects a dynamic formation and dissolution of helix A. The high flexibility of this region can be seen also in Figure 5 where we show the root-mean-square fluctuation (RMSF) of residues as measured over the last 120 μs of our simulations. Consistent with earlier work[9] we find an increased flexibility and partial unwinding of helix B, and to a lesser degree for helix C, for all four systems, and only small differences between control and complex with RNA, see Table 2.

Table 2: Average frequency of helicity in the three regions corresponding to helix A, B and C in the PDB structure. Data are for the complexes and the controls and are averages over all trajectories, with the measurements taken for the last 120 μs. Standard deviations are given in brackets.

helix	129M-178D		129V-178D	
	control	with RNA	control	with RNA
helix A (143-154)	46 (21)	46 (12)	48 (9)	42 (20)
helix B (172-196)	58 (20)	51 (10)	69 (9)	69 (10)
helix C (200-229)	72 (5)	70 (9)	68 (8)	61 (14)
	129M-178N		129V-178N	
	control	with RNA	control	with RNA
helix A (143-154)	41 (15)	35 (7)	27 (23)	27 (17)
helix B (172-196)	65 (9)	57 (18)	68 (17)	60 (12)
helix C (200-229)	66 (12)	68 (9)	65 (9)	68 (8)

* Data are for complexes where the RNA fragment binds to either site 1 or site 3.

Earlier studies have suggested that a fourth α-helix might be formed by residues 109-122,[48] but this helix has not be observed in NMR experiments. On the contrary, when synthesized as a peptide, the 14-residue fragment assumes a β-strand configuration and forms amyloids. In our simulations, we observe transient appearance of this helix for the 106-114 fragment with about 30% in the 129M-178D wild-type variant but only with about 23% in the 129V-178D variant. These frequencies do not depend on binding of the RNA fragment. On the other hand, this helix is seen in the 129M-178N mutant over the whole trajectory with a frequency of about 45%, whereas for the prion-RNA complex the helix

unraveled in most cases after 320 μs, reducing the frequency of this helix from 47% to 25%. A similar behavior is seen for the 129V-178N mutant where the helix occurrence is decreased even more by the presence of RNA from 33%-45% to 10%.

Appearance of this fourth helix is competing with that of strand-like motifs in the 109-122 fragment, with the most frequently observed strands being segments of residues 115-117 and 120-122. Occurrence of the 115-117 β-strand in the last 120 μs is about 30% in 178D variants, regardless of the presence or RNA. However, for the 178N mutants the occurrence of this strand decreases for the complex: for 129V-178N from 45% in the control to 33% with RNA binding, and from 44% to 17% for 129M-178N. On the other hand, binding with RNA increases the frequency of the 120-122 strand from 10%-30% to about 35%-40%. The competition of secondary structural elements is consistent with low-resolution spectroscopy data which indicate that the hydrophobic AGAAAAGA motif of residues 113-120 is metastable and adopt multiple discrete conformations.[49,50] Note that this palindromic sequence is known to form β-sheet-rich neurotoxic fibrils.[51] In high resolution X-ray crystal structures of human PrP in complex with a selective nanobody form the hydrophobic residues 118-122 a β-strand while the following residues 128 to 225 share a fold that is very similar to the corresponding NMR models.[52] Hence, the strandness seen in our simulations for the 109-122 segment in conjunction with the above mentioned experiments indicates that appearance of transient β-strands in this region is a crucial step in the conversion of the prions proteins. Note that the frequencies of strandness for this segment 109-122 are much larger than what is seen in the N-terminus of the protein (the first 100 residues). Here the strandness of isolated prions with 129M is about 7%, and 11%-13% for the 129V variant. Consistent with our earlier work in Ref.,[9] we observe a larger propensity of β-like structure formation with the M129V residue alteration. Upon binding with RNA these frequencies increase for the 178D variants by about 2%, but decrease by a similar amount for 178D.

The overall gain of strandness, when comparing the last 120 μs to the start configuration,
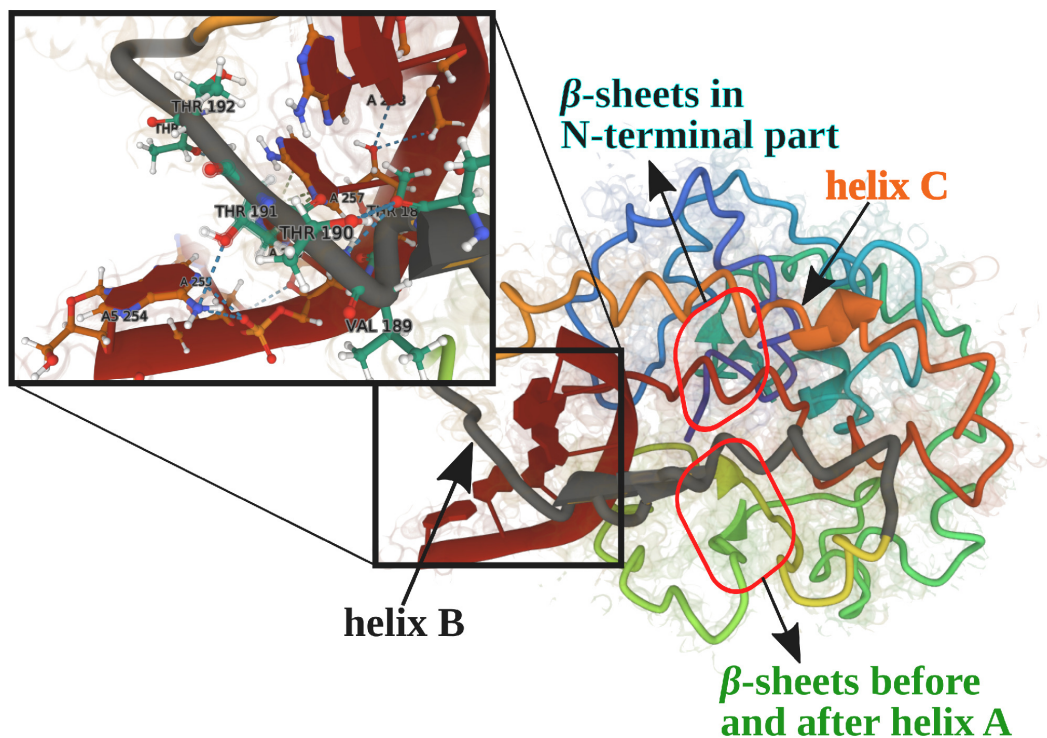
Figure 6: The final structure of the 129M-178N prion-RNA complex for trajectory 2. The prion chain is colored from blue to red from the N- to the C-terminus, respectively, except for helix B, which is dark grey. There is a partial unwinding of helix B in its C-terminal part, caused by the interactions with RNA molecule (shown in magnification). The RNA molecule is drawn in brown. The picture was made using Mol*.[53]

is about 8% for the 129M-178D wild type. While the frequency is here independent of binding of RNA, we see for the other three systems that binding with RNA leads to a gain in strandness: from about 8% to 10%. However, this small number for the gain in strandness is misleading. Our above discussion of the 109-122 segment showed already that strand-like motifs can appear locally with much larger frequencies. Typical strand-like motifs observed in our simulations are shown in Figure 6 where we show the final configuration of the 129M-178N prion-RNA complex in trajectory 2. These small strand and hairpin-like segments are likely the seed for the conversion to the scrapie form PrP^{SC}.

Besides the segment of residues 109-122, β-strands are observed with high frequencies also before the N-terminus of helix A, residues 125-142. For the controls is the strandness

in the last 120 μs higher in prions with methionine in position 129 (37% for 129M-178D and and 31% for 129M-178N) than for 129V-178D and 129V-178N (18% and 29%, respectively). Binding to RNA reduces the differences between the prion variants, and strandness in this segment is now observed for all four systems with about 30% frequency. Another substantial increase of strandness is observed in the region between helix A and B (residues 158-166) where in the last 120 μs the frequency of β-sheet occurrence in the mutants (178N) is more than 40% in both the complex and the control, whereas for 129V-178D wild type the frequency is about 30% and for the 129M-178D complex - 21%. Most commonly seen is a β-strand made of residues 159-163, which is seen with about 30% for the 178D wild types in complex with RNA, and 40% (129V-178N) and 55% in 129M-178N mutant in complex with RNA. The 129M-178N complex is also characterized by the highest strandness in region between helix B and C (residues 190-200). It increases during simulations and in the last 120 μs is 26%, while only 5% -10% for the the other three systems in complex with RNA, with two strands observed: the segment 190-192 and 195-197. Note that these two strands are not found in the control simulations where the average strandness in this region is smaller than 2%.

To more fully understand how the binding of the RNA fragment interacts with the variations of the prion sequence, we show in Fig. 7 the residue-wise RMSF only for the controls (i.e., in absence of poly-A-RNA). This plot shows that the D178N mutation causes higher flexibility in 100-140 region, whereas the alteration M129V raises the flexibility in the 140-190 region. The first region, residues 100-140, contains both the transient helix, seen for the fragment 106-114, and the region of residues 125-140, where we saw a higher propensity for strandness. Analyzing the frequency of contacts between residue 178 and residues between 106-140, we find for the 129M-178D wild type such contacts with a frequency of 1%. This frequency increases to 5% for the 129M-178N mutant, and is diminishing small in all cases where residue 129 is a valine. In the presence of RNA, the frequency of these contacts in-
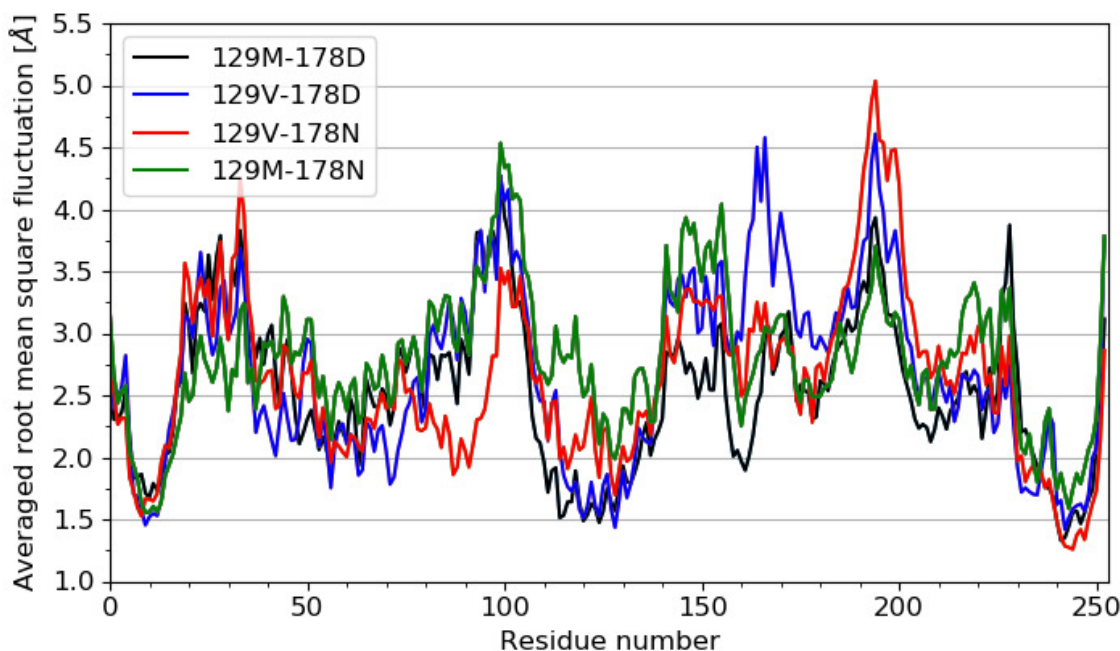
20

Figure 7: RMSF values measured for residues in control simulations of the prion proteins: 129M-178D and 129V-178D wild type variants, and the mutants: 129V-178N and 129M-178N, measured for the last 120 μs, average over all trajectories.

creases to 2% for the 129M-178D wild type, stays at 5% for the 129M-178N mutant, and are now also observed with on average 2% for the 129V-178N mutant. Hence, while in the 129M-178D wild type the position of residue 178 is constraint by electrostatic interactions, the neutral 178N is more flexible and forms more easily contacts, with a more broader distribution of residues, in this region. This raises not only the flexibility of this segment, but also increases the probability of contacts that stabilize the transient helix 106-114, or the strand-like segments in the segment 125-140. Formation of such contacts, however, depends on residue 129 being a methionine. When RNA is bound to the prion at the pincer-forming binding site 1 and 3, do the contacts between prion and RNA ease the formation of such contacts and allow them to form even for the 129V-178N mutant (but with lower probability). Note that 178N can also form contacts with helix A and the following residues 155-165 that destabilizes this helix, but the large fluctuations over the various trajectories makes it difficult to quantify the frequencies. Formation of these contacts is eases when residues 129

21

is a valine or RNA interacts with the prion protein at sites 1 or 3.

On the other hand, the alteration M129V raises the flexibility in 140-200 region, which contains helix A (residues 140-155) and helix B (172-196). Contacts of residue 129 with helix A are rarely observed. Contacts of residue 129 with helix B are located in the N-terminal part (residues 172-190), and seen with about 5%-6% for each residue when residue 129 is a methionine, and 2%-3% when it is a valine, with the frequencies not depending on the type of residue 178. These contacts appear to disturb helix B as the helicity of the helix B region is higher in all variants with a valine as residue 129. However, these contacts are seen only with diminishing probability once RNA binds to either site 1 or 3, and now replaced by contacts between the RNA and helix B which also reduce the stability of this helix. Residue 129 forms most of its contacts with the segment of residues 156-171, connecting helix A and helix B. When a methionine, residues in this segment have such contacts with about 10%-12%, with the frequency not depending on type of residue 178 or presence of RNA. On the other hand, for 129V are contacts in the wild type (178D) only formed with about 3%-4% for each residues in this segment, and with 8%-9% in the mutant D178N. In both cases increases the frequency of such contacts when RNA binds to the prion (to 9% and 14%, respectively). Accordingly, we observe decreased flexibility of the conformations for residues 160-200. For instance, we observe a lower RMSF for the 129M-178D wild type variant in 180-200 region (Fig. 5a), which is due to the large number of contacts with RNA in this region (Fig. 3a). Similar relationships are also seen for the other systems, with the decrease in flexibility smallest for the 129M-178N mutant. Hence, binding with RNA partially compensates for the increase of flexibility seen for the M129V variants. This is consistent with our observation that the strandness in the segment 156-171, which in absence of RNA is larger in the variant with methionine as residue 129 (14% vs 8%-9% in 129V variants), increases in 129V variants when RNA binds to site 1 or 3 (to 18% and 12% for the 129V-178D wild type variant and the 129M-178N mutant, respectively).

22

4 CONCLUSIONS

Extending previous studies by more than a factor thousand we have studied the effect of poly-adenosine RNA and prion sequence on the early stages in the conversion of PrP^C (the functional form of prions) into the toxic and self-replicating PrP^{SC}. Our simulations rely on the UNRES force field and compare the wild type variants 129M-178D and 129V-178D with the corresponding mutants 129M-178N and 129V-178N, either as isolated proteins or with poly-adenosine RNA bound to it. Our simulations confirm earlier observations on the importance of a pincer-like motif between helix A and the poly-basic domain that encapsulates the RNA. This motif is formed after binding of the RNA to either the poly-basic segment of residues 21–31 (binding site 1) or the segment 141–155 (binding site 3). As in earlier work we see an increased flexibility for helix A.

In addition, we see now also strong binding to helix B and C, and observe not only a transient helix in the segment of residues 109-122, but also notice a weakening of all three helices; and the appearance of transient short β-strands that may indicate the start of the conversion to the scrapie form PrP^{SC}. These strands appear in well defined regions at the N-terminal of helix A, or in the helices-connecting loops. The frequency and length of these segments will likely increase as the three helices A, B and C further weaken. Note that we observe in our simulations with the appearance of the strand-like segments also contacts within residues 118-122, and such between the segments 125-130 and 160-170, that are seen also in a recently resolved structure of mammalian prion fibril in its infectious form (PDB-ID: 7LNA). In this model are the chains assembled with parallel in-register intermolecular β sheets.[54] and the above contacts may be crucial for formation of middle β-arch and Greek key in PrP^{Sc}. We observed also a tendency to create contacts between residues 170-190 and 210-220, which can be crucial for formation of disulfide β-arch in PrP^{Sc}, but they are weak.

The above described contacts, seen also in the 7LNA model of an infectious prion fibril,

are observed with higher frequency for the 178N mutants and upon binding with RNA. Similarly, both the weakening of the helices and appearance of the strand-like segments depends on the sequence of the prions and the contacts formed with the poly-adenosine RNA. The D178N mutation causes higher flexibility in 100-140 region, increasing the probability of contacts that stabilize the transient helix 106-114, or the strand-like segments in the segment 125-140, and weakens helix A. When RNA is bound to the Prion at the pincer-forming binding site 1 and 3, do the contacts between prion and RNA ease the formation of such contacts. On the other hand, the alteration M129V raises the flexibility in the 140-190 region which contains both helices B and C. However, this effect is partially compensated by the binding with RNA, which encourages contacts of residue 129 with residues in the loops connecting helices A and B, and helices B-C, stabilizing the transient strands seen in these regions. Hence, binding with poly-A-RNA eases the formation of such contacts formed by residues 129 and 178 that stabilize β-strands and weaken the helices.

While our investigation covers a 1000 times larger time span than our earlier work, we could still only observe the first steps in the conversion of the native PrP^C structure into the scrapie form PrP^{SC}. In future work we will try to extend this investigation, using newly developed multiscale techniques[55] to cover an even larger time scale. We hope that such investigations will allow us to go beyond the mere appearance with the appearance of the transient β-strands and to unveil the next steps in the conversion.

Acknowledgement

References

(1) Prusiner, S. B. Prions. *Proc. Natl. Acad. Sci. U. S. A.* **1998**, *95*, 13363–13383.

(2) Bremer, J.; Baumann, F.; Tiberi, C.; Wessig, C.; Fischer, H.; Schwarz, P.; Steele, A.; Toyka, K.; Nave, K.-A.; Weis, J. et al. Axonal prion protein is required for peripheral myelin maintenance. *Nat. Neurosci.* **2010**, *13*, 310–318.

(3) Frau-Méndez, M.; Fernández-Vega, I.; Ansoleaga, B.; Blanco, R.; Carmona, M.; Río, J.; Zerr, I.; Llorens, F.; Zarranz, J.; Ferrer, I. Fatal familial insomnia: Mitochondrial and protein synthesis machinery decline in the mediodorsal thalamus. *Brain Pathol.* **2017**, *27*, 95–106.

(4) Saá, P.; Harris, D. A.; Cervenakova, L. Mechanisms of prion-induced neurodegeneration. *Expert Rev. Mol. Med.* **2016**, *18*, e5.

(5) Golanska, E.; Sieruta, M.; Corder, E.; Gresner, S. M.; Pfeffer, A.; Chodakowska-Zebrowska, M.; Sobow, T. M.; Klich, I.; Mossakowska, M.; Szybinska, A. et al. The prion protein M129V polymorphism. *Prion* **2013**, *7*, 244–247.

(6) Deleault, N. R.; Harris, B. T.; Rees, J. R.; Supattapone, S. Formation of native prions from minimal components in vitro. *Proc. Natl. Acad. Sci. U. S. A.* **2007**, *104*, 9741–9746.

(7) Miller, M.; Geoghegan, J.; Supattapone, S. Dissociation of Infectivity from Seeding Ability in Prions with Alternate Docking Mechanism. *PLoS Pathog.* **2011**, *7*, e1002128.

(8) Deleault, N.; Lucassen, R.; Supattapone, S. RNA molecules stimulate prion protein conversion. *Nature* **2003**, *425*, 717–720.

(9) Alred, E.; Lodangco, I.; Gallaher, J.; Hansmann, U. H. E. Mutations Alter RNA-Mediated Conversion of Human Prions. *ACS Omega* **2018**, *3*, 3936–3944.

(10) Berhanu, W.; Jiang, P.; Hansmann, U. H. E. In *Computational Methods to Study the Structure and Dynamics of Biomolecules and Biomolecular Processes: From Bioinformatics to Molecular Quantum Mechanics*; Liwo, A., Ed.; Springer International Publishing: Cham, 2019; pp 257–280.

(11) Hansmann, U. H. E.; Okamoto, Y. Prediction of peptide conformation by multicanonical algorithm: New approach to the multiple-minima problem. *J. Comput. Chem.* **1993**, *14*, 1333–1338.

(12) Hansmann, U. H. Parallel tempering algorithm for conformational studies of biological molecules. *Chem. Phys. Lett.* **1997**, *281*, 140–150.

(13) Kmiecik, S.; Gront, D.; Kolinski, M.; Wieteska, L.; Dawid, A. E.; Kolinski, A. Coarse-Grained Protein Models and Their Applications. *Chem. Rev.* **2016**, *116*, 7898–7936.

(14) Han, W.; Wan, C.-K.; Wu, Y.-D. PACE Force Field for Protein Simulations. 2. Folding Simulations of Peptides. *J. Chem. Theory Comput.* **2010**, *6*, 3390–3402.

(15) Liwo, A.; Baranowski, M.; Czaplewski, C.; Gołaś, E.; He, Y.; Jagieła, D.; Krupa, P.; Maciejczyk, M.; Makowski, M.; Mozolewska, M. A. et al. A Unified Coarse-Grained Model of Biological Macromolecules Based on Mean-Field Multipole-Multipole Interactions. *J. Mol. Model.* **2014**, *20*, 2306.

26

(16) Zhou, R.; Maisuradze, G.; Suñol, D.; Todorovski, T.; Macias, M.; Xiao, Y.; Scheraga, H. A.; Czaplewski, C.; Liwo, A. Folding kinetics of WW domains with the united residue force field for bridging microscopic motions and experimental measurements. *Proc. Natl. Acad. Sci. U. S. A.* **2014**, *111*, 18243–18248 .

(17) Rojas, A.; Maisuradze, N.; Kachlishvili, K.; Scheraga, H. A.; Maisuradze, G. G. Elucidating Important Sites and the Mechanism for Amyloid Fibril Formation by Coarse-Grained Molecular Dynamics. *ACS Chem. Neurosci.* **2017**, *8*, 201–209 .

(18) Rojas, A. V.; Maisuradze, G. G.; Scheraga, H. A. Dependence of the Formation of Tau and AB Peptide Mixed Aggregates on the Secondary Structure of the N-Terminal Region of AB. *J. Phys. Chem. B* **2018**, *122*, 7049–7056.

(19) Linh, N.; Krupa, P.; Nguyen, M.; Quang Linh, H.; Li, M. S. Structure and Physicochemical Properties of AB42 Tetramer: Multi-Scale Molecular Dynamics Simulations. *J. Phys. Chem. B* **2019**, *123*, 7253–7269.

(20) He, Y.; Maciejczyk, M.; Ołdziej, S.; Scheraga, H. A.; Liwo, A. Mean-Field Interactions between Nucleic-Acid-Base Dipoles can Drive the Formation of a Double Helix. *Phys. Rev. Lett.* **2013**, *110*, 098101.

(21) Liwo, A.; Czaplewski, C.; Sieradzan, A.; Lubecka, E.; Lipska, A.; Golon, L.; Karczyńska, A.; Krupa, P.; Mozolewska, M.; Makowski, M. et al. *Scale-consistent approach to the derivation of coarse-grained force fields for simulating structure, dynamics, and thermodynamics of biopolymers*; 2020; Vol. 170; pp 73–122.

(22) Sieradzan, A.; Giełdoń, A.; Yin, Y.; He, Y.; Scheraga, H. A.; Liwo, A. A new protein nucleic-acid coarse-grained force field based on the UNRES and NARES-2P force fields. *J. Comput. Chem.* **2018**, *39*, 2360–2370 .

(23) Caughey, B. W.; Dong, A.; Bhat, K. S.; Ernst, D.; Hayes, S. F.; Caughey, W. S. Secondary structure analysis of the scrapie-associated protein PrP 27-30 in water by infrared spectroscopy. *Biochemistry* **1991**, *30*, 7672–7680.

(24) Pan, K. M.; Baldwin, M.; Nguyen, J.; Gasset, M.; Serban, A.; Groth, D.; Mehlhorn, I.; Huang, Z.; Fletterick, R. J.; Cohen, F. E. Conversion of alpha-helices into beta-sheets features in the formation of the scrapie prion proteins. *Proc. Natl. Acad. Sci. U. S. A.* **1993**, *90*, 10962–10966 .

(25) Roy, A.; Kucukural, A.; Zhang, Y. I-TASSER: A unified platform for automated protein structure and function prediction. *Nat. Protoc.* **2010**, *5*, 725–738.

(26) Yang, J.; Yan, R.; Roy, A.; Xu, D.; Poisson, J.; Zhang, Y. The I-TASSER Suite: protein structure and function prediction. *Nat. Methods* **2015**, *12*, 7–8.

(27) Fiser, A.; Šali, A. *Macromolecular Crystallography, Part D*; Methods in Enzymology; Academic Press, 2003; Vol. 374; pp 461–491.

(28) Case, D.; Betz, R.; Cerutti, D.; Cheatham, T.; Darden, T.; Duke, R.; Giese, T.; Gohlke, H.; Götz, A.; Homeyer, N. et al. Amber 16, University of California, San Francisco. 2016.

(29) Trott, O.; Olson, A. J. AutoDock Vina: improving the speed and accuracy of docking with a new scoring function, efficient optimization, and multithreading. *J. Comput. Chem.* **2010**, *31*, 455–461.

(30) Alred, E. J.; Nguyen, M.; Martin, M.; Hansmann, U. H. E. Molecular dynamics simulations of early steps in RNA-mediated conversion of prions. *Protein Sci.* **2017**, *26*, 1524—1534.

(31) Maier, J.; Martinez, C.; Kasavajala, K.; Wickstrom, L.; Hauser, K.; Simmerling, C. ff14SB: Improving the Accuracy of Protein Side Chain and Backbone Parameters from ff99SB. *J. Chem. Theory Comput.* **2015**, *11*, 3696–3713.

(32) Galindo-Murillo, R.; Robertson, J.; Zgarbová, M.; Sponer, J.; Otyepka, M.; Jurecka, P.; Cheatham, T. Assessing the Current State of Amber Force Field Modifications for DNA. *J. Chem. Theory Comput.* **2016**, *12*, 4114–4127.

(33) Rakowski, F.; Grochowski, P.; Lesyng, B.; Liwo, A.; Scheraga, H. A. Implementation of a Symplectic Multiple-Time-Step Molecular Dynamics Algorithm, Based on the United-residue Mesoscopic Potential Energy Function. *J. Chem. Phys.* **2006**, *125*, 204107.

(34) Khalili, M.; Liwo, A.; Jagielska, A.; Scheraga, H. A. Molecular dynamics with the united-residue model of polypeptide chains. II. Langevin and Berendsen-bath dynamics and tests on model α-helical systems. *J. Phys. Chem. B* **2005**, *109*, 13798–13810.

(35) Liwo, A.; Wawak, R. J.; Scheraga, H. A.; Pincus, M. R.; Rackovsky, S. Calculation of protein backbone geometry from α-carbon coordinates based on peptide-group dipole alignment. *Protein Sci.* **1993**, *2*, 1697–1714.

(36) Jorgensen, W. L. Revised TIPS for simulations of liquid water and aqueous solutions. *J. Chem. Phys.* **1982**, *77*, 4156–4163.

(37) Ryckaert, J.-P.; Ciccotti, G.; Berendsen, H. Numerical-Integration of Cartesian Equations of Motion of a System with Constraints – Molecular-Dynamics of N-Alkanes. *J. Comput. Phys.* **1977**, *23*, 327–341.

(38) Essmann, U.; Perera, L.; Berkowitz, M.; Darden, T.; Lee, H.; Pedersen, L. A Smooth Particle Mesh Ewald Method. *J. Chem. Phys.* **1995**, *103*, 8577.

(39) Götz, A.; Williamson, M.; Xu, D.; Poole, D.; Grand, S.; Walker, R. Routine Microsecond Molecular Dynamics Simulations with AMBER on GPUs. 1. Generalized Born. *J. Chem. Theory Comput.* **2012**, *8*, 1542–1555.

(40) Salomon Ferrer, R.; Götz, A.; Poole, D.; Grand, S.; Walker, R. Routine Microsecond Molecular Dynamics Simulations with AMBER on GPUs. 2. Explicit Solvent Particle Mesh Ewald. *J. Chem. Theory Comput.* **2013**, *9*, 3878–3888.

(41) Alonso, D. O. V.; An, C.; Daggett, V. Simulations of Biomolecules: Characterization of the Early Steps in the pH-Induced Conformational Conversion of the Hamster, Bovine and Human Forms of the Prion Protein. *Philos. Trans.: Math., Phys. Eng. Sci.* **2002**, *360*, 1165–1178.

(42) Makowski, M.; Liwo, A.; Scheraga, H. A. Simple Physics-Based Analytical Formulas for the Potentials of Mean Force of the Interaction of Amino Acid Side Chains in Water. VII. Charged-Hydrophobic/Polar and Polar-Hydrophobic/Polar Side Chains. *J. Phys. Chem. B* **2017**, *121 2*, 379–390.

(43) Yin, Y.; Sieradzan, A.; Liwo, A.; He, Y.; Scheraga, H. A. Physics-Based Potentials for Coarse-Grained Modeling of Protein–DNA Interactions. *J. Chem. Theory Comput.* **2015**, *11*, 1792–1808.

(44) Lubecka, E.; Liwo, A. A general method for the derivation of the functional forms of the effective energy terms in coarse-grained energy functions of polymers. II. Backbone-local potentials of coarse-grained O $1 \rightarrow 4$ -bonded polyglucose chains. *J. Chem. Phys.* **2017**, *147*, 115101.

(45) Liwo, A.; Czaplewski, C.; Sieradzan, A. K.; Lubecka, E. A.; Lipska, A. G.; Łukasz Golon,; Karczyńska, A.; Krupa, P.; Mozolewska, M. A.; Makowski, M. et al. In *Computational Approaches for Understanding Dynamical Systems: Protein Folding and As-*

sembly; Strodel, B., Barz, B., Eds.; Progress in Molecular Biology and Translational Science; Academic Press, 2020; Vol. 170; pp 73–122.

(46) Tian, C.; Kasavajhala, K.; Belfon, K. A. A.; Raguette, L.; Huang, H.; Migues, A. N.; Bickel, J.; Wang, Y.; Pincay, J.; Wu, Q. et al. ff19SB: Amino-acid specific protein backbone parameters trained against quantum mechanics energy surfaces in solution. *J. Chem. Theory Comput.* **2019**, *16*, 528–552.

(47) Biljan, I.; Giachin, G.; Ilc, G.; Zhukov, I.; Plavec, J.; Legname, G. Structural basis for the protective effect of the human prion protein carrying the dominant-negative E219K polymorphism. *Biochem. J.* **2012**, *446*, 243–251.

(48) Gasset, M.; Baldwin, M. A.; Lloyd, D. H.; Gabriel, J. M.; Holtzman, D. M.; Cohen, F.; Fletterick, R.; Prusiner, S. B. Predicted alpha-helical regions of the prion protein when synthesized as peptides form amyloid. *Proc. Natl. Acad. Sci. U. S. A.* **1992**, *89*, 10940–10944 .

(49) Kuwata, K.; Matumoto, T.; Cheng, H.; Nagayama, K.; James, T. L.; Roder, H. NMR-detected hydrogen exchange and molecular dynamics simulations provide structural insight into fibril formation of prion protein fragment 106-126. *Proc. Natl. Acad. Sci. U. S. A.* **2003**, *100*, 14790–14795.

(50) Lim, K. H.; Nguyen, T. N.; Damo, S. M.; Mazur, T.; Ball, H. L.; Prusiner, S. B.; Pines, A.; Wemmer, D. E. Solid-state NMR structural studies of the fibril form of a mutant mouse prion peptide PrP89–143(P101L). *Solid State Nucl. Magn. Reson.* **2006**, *29*, 183–190.

(51) Forloni, G.; Angeretti, N.; Chiesa, R.; Monzani, E.; Salmona, M.; Bugiani, O.; Tagliavini, F. Neurotoxicity of prion protein fragment. *Nature* **1993**, *362*, 543–546.

(52) Abskharon, R. N. N.; Giachin, G.; Wohlkonig, A.; Soror, S. H.; Pardon, E.; Leg-name, G.; Steyaert, J. Probing the N-terminal beta-sheet conversion in the crystal structure of the human prion protein bound to a nanobody. *J. Am. Chem. Soc.* **2014**, *136*, 937–944 .

(53) Sehnal, D.; Bittrich, S.; Deshpande, M.; Svobodová, R.; Berka, K.; Bazgier, V.; Velankar, S.; Burley, S. K.; Koča, J.; Rose, A. S. Mol* Viewer: modern web app for 3D visualization and analysis of large biomolecular structures. *Nucleic Acids Res.* **2021**, *49*, W431–W437 .

(54) Kraus, A.; Hoyt, F.; Schwartz, C.; Hansen, B.; Artikis, E.; Hughson, A.; Raymond, G.; Race, B.; Baron, G.; Caughey, B. High-resolution structure and strain comparison of infectious mammalian prions. *Mol. Cell* **2021**, *81*, 4540-4551.

(55) Yasar, F.; Ray, A. J.; Hansmann, U. H. E. Resolution exchange with tunneling for enhanced sampling of protein landscapes. *Phys. Rev. E* **2022**, *106*, 015302 .

Graphical TOC Entry